A simplified reinforcing steel model suitable for cyclic loading including ultra-low-cycle fatigue effects

Luís A.M. Mendes[a], Luís M.S.S. Castro[a,b]

[a]*Instituto de Engenharia de Estruturas, Território e Construção, Av. Rovisco Pais 1, 1049-001 Lisboa, Portugal*
[b]*Instituto Superior Técnico, Universidade de Lisboa, Av. Rovisco Pais 1, 1049-001 Lisboa, Portugal*

Abstract

This paper presents a new constitutive model for the simulation of reinforcing steel bars used in common reinforced concrete structures and it is designed to be used for general loading cases. The model includes the well-known Guiffrè-Menegotto-Pinto softened branch, although new expressions are proposed for the evolutions of the curvature-related parameter and of the yield surface. The constitutive relation is enhanced with an innovative and simplified proposal for considering ultra-low-cycle fatigue effects. This phenomenon is particularly important for structures that undergo a small number of very large displacement cycles, *e.g.* when subjected to intense seismic events. It is known that in those situations the steel reinforcements experience a continuum and significant strength decrease that ultimately leads to premature failure induced by fatigue.

The model's mathematical description and some relevant implementation issues are described. Its accuracy is assessed by means of a series of validation tests using experimental data available in the bibliography.

Keywords: Concrete Reinforcing Steel, Constitutive Model, Cyclic Response, Ultra-Low-Cycle Fatigue, Finite Element Method

1. Introduction

It is generally accepted that steel reinforcements have a predominant effect on the hysteretic response of properly designed *reinforced concrete* (RC) members. Naturally, this implies that

Email address: luis.marcos.mendes@tecnico.ulisboa.pt (Luís A.M. Mendes)

the accuracy of the steel reinforcement simulation within numerical models is determinant to the quality of the results.

The reinforcing steel monotonic response is reasonably easy to be simulated with accuracy when the initial elastic response, the yielding plateau, when present, and the strain-hardening branch are properly simulated (see Figure 1a). On the other hand, the response under cyclic and alternating loading is more challenging due to the complexity associated with several simultaneous effects. The unloading and reloading branches are characterized by a stiffness similar to the one occurring at first loading. Moreover, the response is influenced by two additional phenomena: After experiencing plastic deformation the stress-strain response after reversal presents the so-called *Bauschinger effect*, which is associated with the anticipation of the departure from the elastic stiffness after reversal (see Figure 1b). Secondly, the response experiences a combination of kinematic hardening (elastic range translation) and isotropic hardening (elastic range expansion/contraction).

Another significant material phenomenon is the so-called ultra-low-cycle fatigue. This effect occurs when the steel reinforcements experience large inelastic cyclic deformations, which can be caused by earthquake-induced forces, and results into significant steel resistance degradation that may lead to collapse by fracture at much lower stress levels than for the virgin material. Although this effect is often disregarded in modelling and design situations, a significant number of studies were carried out recently, *e.g.* studies with different classes of steel [28, 13] and on the interaction with other effects like corrosion [2]. In addition, several fatigue-life models have been proposed over the years, *e.g.* the Coffin-Mason model [6, 23], the Koh-Stephens model [17] and the Mander-Panthaki model [22].

After calibration, these models can predict with sufficient accuracy the effect of low-cycle fatigue on the reinforcements. Nevertheless, these fatigue-life models are usually defined in terms of total or plastic strain with the number of cycles to failure, thus the direct implementation on constitutive models to be incorporated in finite element models is not straightforward.

This paper tries to mitigate this problem by proposing a simplified model that can simulate the main aspects of the phenomena described before, with particular focus on the ultra-low-cycle fatigue effect, defined in this case for less than 50 full cycles with plastic deformation.

Other effects are not included due to the limited impact they would have on the accuracy of the simulation or to simplify the formulation and improve the computational efficiency of the model. These are the cases of the clear yield plateau observed on mild steel bars, of buckling on compressed bars and of asymmetric response under alternating tension and compression forces. Furthermore, strain-rate effects for dynamic loading are also not considered and all material parameters should be obtained from *quasi*-static tests. Nevertheless, the parameters may be tuned to improve the simulation accuracy for dynamic analyses, *e.g.* by adjusting the yield stress value.

2. Low-cycle fatigue

Fatigue can be seen as the process that leads to damage or to failure of a structural member due to repeated loading. In particular, low-cycle fatigue develops when this phenomenon occurs with a relative small number of cycles. In contrast, medium-cycle and high-cycle fatigue occurs for a larger number of cycles, generally between 10^3 to 10^8 cycles. This last type is mostly associated with service loading and is being studied for several decades, *e.g.* see Tilly's review on steel reinforcement fatigue [32]. Some examples of civil engineering structures that require specific studies on the fatigue effect are bridges subjected to traffic or to intense thermal loads [30, 29] and high-rise buildings or wind turbines, and their components, when excited by wind loads [14, 15].

The fatigue-life curve of a material can be defined as the number of cycles N_c required to produce a fatigue failure for a given stress or strain amplitude. According to Brown and Kunnath [4], for an engineering alloy (*e.g.* steel) this curve takes the form represented in Figure 2. When loading amplitude is large, but below the ultimate strength for a single load application, there will be inelastic deformation and failure occurs after a reduced number of cycles, typically under 1000 (low-cycle fatigue). On the other hand, elastic deformation will occur when the loading amplitude is small and the number of cycles required to produce fatigue failure is very large, often in the order of millions (high-cycle fatigue). For very small loading amplitudes, fatigue will not occur or the number of cycles to induce failure is so large that this phenomenon is neglected.

Fatigue develops by the damage generated and by the creation and propagation of fatigue cracks due to the effect of repeated loading. Ultimately, this will lead to failure when the specimen does not have sufficient resistance to withstand the prescribed loading. During this process, cyclic strength and stiffness degradation can be observed in the response of reinforcing steel bars.

One question arises regarding what would be the number of cycles expected to occur during a seismic event. According to Panthaki [26], an earthquake load can result in large tension and compression strains in the reinforcements and between 2 to 10 full cycles for common structures and up to 30 cycles for structures with high natural frequencies (ultra-low-cycle fatigue). Considering this information, it is possible to conclude that this phenomenon is likely to result in cyclic degradation, or even in anticipated reinforcement failure.

3. Modelling

Several models have been proposed to simulate the response of steel bars used in reinforced concrete structures. The most widespread models range from the simpler bilinear or multilinear constitutive relations, *e.g.* the model proposed by Aktan and Karlsson [1] and those with smooth elastic-plastic transition, like the Ramberg-Osgood model [27], the Guiffrè-Menegotto-Pinto model [11, 24] and the models proposed by Mander and co-workers [21, 20, 5], to name a few. In addition, significant developments have been made to capture buckling of longitudinal bars. This research led to several proposals, *e.g.* the models suggested by Monti and Nuti [25], by Gomes and Appleton [12], and more recently by Dhakal and Maekawa [8], all based on the Guiffrè-Menegotto-Pinto model. Another significant innovation was made by Dodd and Restrepo-Posada [9] in the simulation of the asymmetrical behaviour under tension and compression observed in the experiments, by means of the so-called *natural coordinate system*.

This paper presents a new model for the simulation of reinforcing steel bars used in common reinforced concrete structures. The model is designated as *Refined Reinforcing Steel* (RSteel) and consists of a base model and one sub-model. The base model adopts initially a bilinear relation until the first load reversal is reached, followed by a softened branch to simulate the Bauschinger effect. The equation of the softened branch is the well-known Guiffrè-Menego-

tto-Pinto [24] equation improved by Filippou *et al.* [10]. Nevertheless, a new expression is proposed for the evolution of a curvature-related parameter. In addition, the base model adopts a new formulation for the cyclic hardening rule and is complemented by a specific sub-model to simulate the ultra-low-cycle fatigue phenomenon.

3.1. Base model

The *RSteel* model general equation is the following:

$$\sigma_s = E_s \left(\varepsilon_s - \varepsilon_{sp}\right), \tag{1}$$

where ε_{sp} is the plastic strain that can be computed by subtracting the elastic strain from the total strain, using:

$$\varepsilon_{sp} = \varepsilon_s - \frac{\sigma_s}{E_s}. \tag{2}$$

The yield and ultimate strength are computed from:

$$\sigma_{sy} = E_s \varepsilon_{sy}, \tag{3}$$

$$\sigma_{su} = \sigma_{sy} + \beta_0 E_s \left(\varepsilon_{su} - \varepsilon_{sy}\right), \tag{4}$$

where β_0 represents the initial strain-hardening modulus (see Figure 3a).

In the proposed model, the strain-hardening modulus changes throughout the analysis as follows[1]:

$$\beta^{\pm}\left(\varepsilon_{\max}\right) = \begin{cases} \beta_0, & \text{if } \varepsilon_{\max} \leq \varepsilon_{sy} \\ \beta_0 \left(1 - \frac{\varepsilon_{\max} - \varepsilon_{sy}}{\varepsilon_{su} - \varepsilon_{sy}}\right), & \text{if } \varepsilon_{\mathrm{sy}} < \varepsilon_{\max} \leq \varepsilon_{\mathrm{su}} \\ 0, & \text{otherwise} \end{cases}, \tag{5}$$

where $\varepsilon_{\max}$ stores the maximum absolute value of the strain reached previously. This definition implies that $\beta^{\pm}$ changes linearly between β_0 and zero at $\varepsilon_{\max} = \varepsilon_{su}$, as represented in Figure 4a. It

[1]The symbol $\beta^{\pm}$ references both β^{+} and β^{-} which are associated with the positive and negative yield surface, respectively.

should be emphasized that β^+ and β^- are only updated after a negative and positive load reversal, respectively.

The *RSteel* model adopts the following definition for the yield surface[2]:

$$\phi_*^{\pm} = \pm\sigma_{su} \mp \beta^{\pm} E_s \varepsilon_{su} + \beta^{\pm} E_s \varepsilon_s. \tag{6}$$

This definition implies that the positive and negative yield surfaces rotate about the points A^+ or A^-, respectively (see Figure 3b). This allows adding isotropic cyclic hardening to the simulation because the rotation leads to a homothetic expansion of the yield surface in both loading directions.

The adopted equation for the softened branch corresponds to the well-known Guiffrè-Menegotto-Pinto expression [11, 24]:

$$\sigma_s^* = \beta^{\pm}\, \varepsilon_s^* + (1-\beta^{\pm}) \frac{\varepsilon_s^*}{\left\{1 + (\varepsilon_s^*)^R\right\}^{1/R}}, \tag{7}$$

and the enhanced coordinate transformation proposed by Filippou, Popov and Bertero [10] is assumed:

$$\varepsilon_s^* = \frac{\varepsilon_s - \varepsilon_{sa}}{\varepsilon_{s0} - \varepsilon_{sa}},\ \sigma_s^* = \frac{\sigma_s - \sigma_{sa}}{\sigma_{s0} - \sigma_{sa}}, \tag{8}$$

where $(\varepsilon_{sa}, \sigma_{sa})$ represents the strain and stress at the inversion point preceding each branch and $(\varepsilon_{s0}, \sigma_{s0})$ represents the strain and stress at the intersection between the elastic and hardening slopes (see Figure 3b).

For the proposed model, the coordinates $(\varepsilon_{s0}, \sigma_{s0})$ of each softened branch can be computed by equating the envelope curve with the equation of a line with slope E_s passing through $(\varepsilon_{sa}, \sigma_{sa})$:

$$\phi_*^{\pm} = \sigma_{sa} - E_s \varepsilon_{sa} + E_s \varepsilon_s, \tag{9}$$

[2]The symbols $\pm$ and $\mp$ are used to condense two equations. $\pm$ should be substituted by $+$ for the first equation (ϕ_*^+) and by $-$ for the second equation (ϕ_*^-), and *vice-versa* for $\mp$.

leading to:

$$\varepsilon_{s0}^{\pm} = \frac{-\sigma_{sa} + E_s\,\varepsilon_{sa} \mp \beta^{\pm}\,E_s\,\varepsilon_{su} \pm \sigma_{su}}{(1-\beta^{\pm})\,E_s}, \tag{10}$$

$$\sigma_{s0}^{\pm} = \pm\sigma_{su} \mp \beta^{\pm} E_s \varepsilon_{su} + \beta^{\pm} E_s \varepsilon_{s0}. \tag{11}$$

The parameter R in equation (7) is related to the curvature of the transition between the elastic and the hardening branches. To enhance the flexibility and the representativeness of the model, the following alternative definition for the evolution of this parameter is adopted:

$$R\left(\varepsilon_{sp}^{ac}\right)\begin{cases} R_0, & \text{if } \varepsilon_{\text{sp}}^{\text{ac}} \leq \varepsilon_{\text{sy}} \\ \alpha R_0, & \text{if } \varepsilon_{\text{sp}}^{\text{ac}} > \varepsilon_{\text{sy}} \end{cases}, \tag{12}$$

with:

$$\alpha = 1 - c_R\left\{1 - \left(\frac{\exp\left(-\varepsilon_{sp}^{ac}/\varepsilon_{sy}\right)}{\exp\left(-1\right)}\right)^{\frac{n_R}{100}}\right\}, \tag{13}$$

where R_0, c_R, n_R are material parameters to be identified and ε_{sp}^{ac} represents the accumulated plastic strain until the previous load reversal. At the end of n_s load steps, this variable can be computed using:

$$\varepsilon_{sp}^{ac} = \sum_{j=1}^{n_s} \left|\Delta\varepsilon_{sp,j}\right|, \tag{14}$$

where $\Delta\varepsilon_{sp,j}$ represents the plastic strain increment at load step j, which can be easily computed using the values returned by equation (2).

The c_R parameter represents a reduction factor for R and parameter n_R may be used to change the evolution of this reduction. Figure 4b presents the effect of these parameters on the progress of R normalized by its initial value.

3.2. Ultra-low-cycle fatigue sub-model

The most obvious parameters that can feed the model with information about the fatigue induced in the material are the number and the amplitude of the cycles the bar is subjected. However,

under general loading cases, the stress-strain history is not repetitive as in fatigue tests. As a result, alternative state variables must be used for this purpose. The accumulated plastic strain experienced by the bar throughout the loading history $\left(\varepsilon_{sp}^{ac}\right)$ defined in equation (14) is a natural choice. Other parameters may be used, *e.g.* Suidan *et al.* [31] proposed the so-called *Rainflow Cycle Counting method* to compute an equivalent strain amplitude from random strain histories, like the ones resulting from seismic events.

To investigate the feasibility of using the accumulated plastic strain, the experimental data obtained by Brown *et al.* [3, 4] is used. The work developed by these authors consisted of 34 low-cycle fatigue tests with constant amplitude. The tested reinforcements were #6, #7 and #8 bars, which correspond to diameters of 19.1mm, 22.2mm and 25.4mm, respectively. The steel used was Grade 60 with the following mechanical properties: σ_{sy} = 420MPa; σ_{su} = 620MPa; $\varepsilon_{su} = 8\% - 9\%$. More information about these tests are available in the references [3, 4].

The data reported in these publications for the number of cycles at failure are associated with the number of half cycles, instead of the number of full cycles required for the effective failure of the specimen. This data was corrected in order to adopt the quantity N_c^f as the number of full cycles. Table 2 in the Appendix presents a summary of the results reported by Brown *et al.* [4], where ε_a and ε_{ap} represent the strain and the plastic strain amplitudes, and N_c^{cr} and N_c^f the number of cycles when the first fatigue crack is identified and when the specimen failed, respectively.

Figure 5 presents the values of ε_{sp}^{ac} for the tests performed by Brown *et al.* [4]. In this case, the accumulated plastic strain can be computed using the following expression:

$$\varepsilon_{sp}^{ac}\left(N_c\right) = 4\,\varepsilon_{ap}\,N_c, \tag{15}$$

where N_c is either the number of cycles when the first crack is identified or at failure.

This figure shows that this quantity presents some variance and that it is possible to identify what seems to be a linear dependency between ε_{sp}^{ac} and the plastic amplitude of the cycles. This effect is related to the intensity of the plastic deformation for each cycle. For the same level of the accumulated plastic strain, larger plastic amplitudes induce higher fatigue-type damage than smaller plastic amplitudes. This effect represents a loading-related response that is not a material

property, and therefore, should be expunged. To achieve this, the following linear *severity factor* is introduced:

$$s_f = \frac{\Delta\varepsilon^*_{sp}}{\varepsilon_{sy}}, \tag{16}$$

where $\Delta\varepsilon^*_{sp}$ represents the amplitude of the plastic deformation between load reversals and ε_{sy} the monotonic yield stress.

Introducing the severity factor into equation (14), it is possible to obtain the definition of the *corrected accumulated plastic strain*, in this case defined after n_r load reversals:

$$\tilde{\varepsilon}^{ac}_{sp} = \sum_{r=1}^{n_r} \left(\varepsilon^{ac}_{sp}\, s_f\right)_r = \sum_{r=1}^{n_r} \left(\frac{\varepsilon^{ac}_{sp}\, \Delta\varepsilon^*_{sp}}{\varepsilon_{sy}}\right)_r. \tag{17}$$

It is implied in the last equation that $\tilde{\varepsilon}^{ac}_{sp}$ is only updated when a load reversal is identified. Moreover, the possibility of partial unloading should be taken into consideration and an effective reversal should only be considered when the stress changes from tension to compression or *vice versa* (see Figure 8).

Figure 6 presents the same data used for Figure 5 after correcting the accumulated plastic strain using equation (17). In this case, this expression can be simplified into:

$$\tilde{\varepsilon}^{ac}_{sp}(N_c) = \frac{8\,\varepsilon^2_{ap}\,N_c}{\varepsilon_{sy}}. \tag{18}$$

From Figure 6 it is possible to observe that the introduction of the severity factor significantly reduces the dependency on the cycle amplitude observed previously. This can be seen by noting the nearly constant linear regression line, both after the identification of the first crack and at bar failure. Nevertheless, the same level of dispersion in the results is still observed because this mainly originates from dispersion already in the original test results.

The procedure adopted to remove the load amplitude dependency is based on observing what seems to be a linear trend in Figure 5. There is not a well-established physical framework to support this option, other than it is intuitive that larger amplitude plastic strains tend to be more penalizing for the reinforcement than smaller amplitude strains. This approach was adopted due

to its simplicity and because the results obtained showed that the load dependency is significantly reduced for the cases considered.

The results obtained by Mander *et al.* [22, 26] are used for further validation of the proposed ultra-low-cycle fatigue sub-model. In this case, the tests were performed with 5/8in. (15.9mm) bars made of Grade 40 steel, which under monotonic tension tests returned the following results: σ_{sy} = 331MPa; σ_{su} = 565MPa; ε_{su} = 17%.

Similarly to what was done before, Table 3 in the Appendix presents a summary of the experimental results obtained. The failure criterion adopted by Mander *et al.* included a combination of two conditions [22]. For small amplitude cycles $\varepsilon_a < \pm 2\%$, the failure was recognized by monitoring the σ_s^c/σ_s^0 curves (similar to the one presented in Figure 10f) and by identifying when this ratio starts to drop. For larger amplitude cycles, the stress at reversal decreased continuously, so, it is not possible to identify a well-defined saturation level. Consequently, the failure was identified by visual observation of fatigue crack initialization.

The results obtained using the proposed procedure are presented in Figure 7. It can be observed that after removing one outlier value that was clearly out of the general trend, a similar improvement for the load dependency can be observed. This gives a good indication regarding the generality of the adopted formulation.

The introduction of the proposed ultra-low-cyclic fatigue sub-model into the *RSteel* model is made by multiplying the yield surfaces (6) by a fatigue factor defined by:

$$\gamma_f = 1.0 - c_f \left(\frac{\tilde{\varepsilon}_{sp}^{ac}}{\varepsilon_f} \right)^{n_f}, \tag{19}$$

where ε_f is a load independent material property that specifies the value of the corrected accumulated plastic strain $\left(\tilde{\varepsilon}_{sp}^{ac}\right)$ at bar failure. The parameters c_f and n_f control the fatigue evolution.

The parameter c_f defines the amount of degradation before failure. Brown *et al.* [4] concluded from the tests with ϕ19mm bars that independently of the strain amplitude the degradation is gradual and not too intense until the stress at reversal normalized by its value at first loading $\left(\sigma_s^c/\sigma_s^0\right)$ is around 0.75. Consequently, the parameter c_f should present values of about 0.20-0.30 plus the component associated with cyclic hardening. The parameter n_f can be used to change the evolution of the degradation with the corrected accumulated plastic strain. Figure 9

presents the effect of changing this parameter on the fatigue factor.

The steel reinforcement bar is considered to have achieved rupture and γ_f is set to zero, if the following condition is met:

$$\tilde{\varepsilon}_{sp}^{ac} > \varepsilon_f \ \wedge \ \sigma_s > 0, \tag{20}$$

in which the last equation enforces that steel reinforcement rupture can only happen under tensile loading.

If the c_f parameter is set to zero this implies that no degradation occurs before the reinforcement rupture. In addition, by adopting very large values for ε_f the steel reinforcement failure will not occur and the ultra-low-cycle fatigue effect is not considered in the simulation.

Figure 10 presents a comparison between the results of the fatigue tests performed by Brown *et al.* [4] with ϕ19mm bars and the results obtained using the *RSteel* model. Figure 10a to Figure 10e present the results obtained for cycles with strain amplitudes of 1.50%, 1.75%, 2.50% and 3.00%, respectively. All the results were obtained with the following model parameters: E_s = 215GPa; β_1 = 0.5%; σ_{sy} = 540MPa; ε_{su} = 8.5%; and R_0 = 3.0; c_R = 0.5; n_R = 0.5 for the evolution of the softened curve curvature; and ε_f = 21.0; c_f = 0.25; n_f = 1.00 for the fatigue sub-model. These parameters where chosen through a manual optimization process carried out to fit the experimental results.

For the case of the test with strain amplitude of 2.50%, the stress-strain curve is available in the published work by Brown *et al.* [4]. This result is compared side-by-side with the results obtained using the *RSteel* model in Figure 10c and Figure 10d, respectively. A good match can be observed between both data sets. The results could have been even more similar but the goal of using the same parameters for all tests limited the adjusting range for the parameters. Furthermore, the experimental results under compression and tension forces showed some asymmetry and this effect could not be simulated with the proposed model. Using the definition expressed in equation (20) means that the rupture of the bar can happen anywhere under tensile loading. This is visible in the simulations presented in Figure 10.

Figure 10f presents the normalized stress at reversal obtained for all the tests considered. These data are compared with the experimental results published by Brown *et al.* [4]. The

results show that the *RSteel* model and in particular the ultra-low-cycle fatigue sub-model is able to simulate all the test results with very good accuracy and always using the same set of model parameters. This demonstrates that the sub-model is reproducing well the fatigue evolution and the induced failure.

4. Implementation

The *RSteel* model may be used in a variety of applications that are left open at this stage. Possible uses range from the implementation on fibers for cross-section or structural analyses, and also, in the framework of the finite element method. These applications often require the definition of two main procedures: state determination and stiffness matrix computation, either at cross-section or at element level. The state determination procedure is described in Algorithm 1 for incremental analyses and Table 1 compiles the pertinent information regarding the model parameters.

Computing the tangent stiffness matrix requires knowing $\partial\sigma_s/\partial\varepsilon_s$ that can be obtained by applying the chain rule, as follows:

$$\frac{\partial\sigma_s}{\partial\varepsilon_s} = \frac{\partial\sigma_s}{\partial\sigma_s^*}\frac{\partial\sigma_s^*}{\partial\varepsilon_s^*}\frac{\partial\varepsilon_s^*}{\partial\varepsilon_s}. \tag{21}$$

Recalling the relations presented in equation (8), it is possible to obtain:

$$\frac{\partial\sigma_s}{\partial\sigma_s^*} = \sigma_{s0} - \sigma_{sa}, \tag{22}$$

$$\frac{\partial\varepsilon_s^*}{\partial\varepsilon_s} = \frac{1}{\varepsilon_{s0} - \varepsilon_{sa}}, \tag{23}$$

and the remaining term results from equation (7):

$$\frac{\partial\sigma_s^*}{\partial\varepsilon_s^*} = \beta^{\pm} - \frac{\beta^{\pm} - 1}{\left\{1 + (\varepsilon_s^*)^R\right\}^{1+1/R}}. \tag{24}$$

It should be noted that the parameters $\beta^{\pm}$ and R do not depend on ε_s^* because they are only updated after reversal. The complete set of possible values for $\partial\sigma_s/\partial\varepsilon_s$ are listed below for each branch represented in Figure 11a:

$$k = \frac{\partial \sigma_s}{\partial \varepsilon_s} = \begin{cases} E_s, & \text{case 1} \\ \beta_0 E_s, & \text{case 2} \\ \frac{\sigma_{s0}-\sigma_{sa}}{\varepsilon_{s0}-\varepsilon_{sa}} \left\{ \beta^{\pm} - \frac{\beta^{\pm}-1}{\left[1+\left(\varepsilon_s^*\right)^R\right]^{1+1/R}} \right\}, & \text{case 3} \\ 0, & \text{case 4} \end{cases} . \tag{25}$$

Figure 11b presents the parameter R effect on the softened branch slope. It can be observed that increasing values of this parameter leads to sharper slope transitions.

A finite element implementation is straightforward (*e.g.* see Crisfield [7]). Nonetheless, if implemented as a beam element further simplifications are needed or additional models must be included for the other degrees-of-freedom. Special attention should be given to the choice of appropriate state variables, to check for loading and unloading situations and to identify load reversals. Furthermore, the use of the *tangent stiffness matrix* can greatly enhance the computational efficiency of the numerical model by increasing the convergence rate.

5. Validation

The proposed model is validated against experimental results of common reinforcing bars tested under cyclic and alternating loading. Experiments with asymmetric tension-compression cycles were adopted because after concrete cracking the steel reinforcements are more stressed for tensile loading because the concrete ceases to have a predominant contribution.

Figure 12 presents the data from multiple cyclic tests of reinforcing bars compared with the results obtained by feeding the strain history into the *RSteel* model. The model parameters used in each case are presented in Table 4 in the Appendix.

Figure 12a illustrates the experimental results obtained by Kent and Park [16] with mild steel (Grade 275) reinforcing bars manufactured in New Zealand. This test was chosen because it represents a non-alternating cyclic test and in this case the inelastic response is less intense, hence the fatigue effect is less important as proved by obtaining $\gamma_f = 0.99$ at the end of the simulation. Comparing the experimental with the numerical results two issues become evident: Similar to other works (*e.g.* Mander [21]), the simulation was performed with an elasticity modulus smaller than 200GPa to cope with the experimental results that clearly show a relatively

flexible response at first loading and in subsequent unloading and reloading branches. In addition, specimen 19 experienced a smooth transition between the elastic and the elastoplastic branch at first loading, contrary to similar specimens tested in the same test campaign.

The following case concerns the tests carried out by Leslie [18] with high strength steel (Grade 380) also from New Zealand and with a specimen that was subjected to 8 intense cycles with plastic deformation. At the end of the numerical prediction, the parameter γ_f reached the value of 0.90 revealing that the fatigue sub-model is adding significant strength degradation into the simulation. Switching off this sub-model by setting $c_f = 0$ shows that the peak stress values become overestimated, in particular at the end of the test. Moreover, Figure 12b shows some asymmetries in the softened branches for subsequent tension and compression loading cycles, which cannot be predicted by the *RSteel* model. The peak stresses achieved in each cycle are well reproduced by the model.

The tests carried out by Aktan *et al.* [1] are considered in the following two examples. High strength steel manufactured in USA is used and size #9 and #6 bars are chosen. In both cases the results are reasonably well predicted by the model. However, the yield plateau is not captured as a result of the simplifications introduced in the model for the aforementioned reasons. In these two tests, the fatigue-related strength degradation is very significant as demonstrated by retrieving $\gamma_f = 0.75$ and $\gamma_f = 0.84$ at the end of Test 5 and Test 8, respectively. On the other hand, asymmetries in the response under tension and compression forces can be found in the experimental data, which reduces the accuracy of the numerical prediction.

The last group of experiments used Grade 60 steel reinforcing bars from the USA and were published by Ma *et al.* [19]. In these cases the fatigue is low ($\gamma_f > 0.95$) and the RSteel was able to predict the experimental results with good accuracy.

In these validation tests, the parameters adopted for the softened branch curvature ranged between: $R_0 = 1.8-4.0$; $c_R = 0.2-0.6$; $n_R = 0.8-5.0$. One can say from the experience obtained using the model that the R_0 parameter is typical about 2.5 and a reduction of $c_R = 30\% - 40\%$ is expected to occur at failure. This reduction is more intense at the first cycles as proved by using values greater than 1.0 for n_R and normally about 4.0.

In what concerns the ultra-low-cycle fatigue parameters, these ranged in the validation tests

between: $c_f = 0.30 - 0.40; n_f = 0.38 - 0.75$ and ε_f was set to 24.5. As discussed before, ε_f represents the value of $\tilde{\varepsilon}_{sp}^{ac}$ at bar failure. This parameter was set to 24.5 as a result of the processing made with the data obtained by Brown *et al.* [4] and illustrated in Figure 6. From the experience obtained by authors, values between 20.0 to 25.0 seem adequate for this parameter. Setting the strength reduction to $c_f = 30\%-40\%$ at bar failure represents a common situation and values less than 1.00 are commonly adopted for n_f, which implies that most of this degradation occurs at the first cycles.

Taking into consideration the results presented, it can be stated that very good predictions for the experimental results are obtained using the *RSteel* model. This demonstrates the flexibility of the proposed model and the adjustment to the effective behaviour of the steel reinforcing bars. Nevertheless, it is possible to observe minor differences in some cases for the stress at reversal and for softened branch curvature. In addition, some asymmetries can be identified in tests carried out with alternating tensile and compressive forces. This type of behaviour is not too significant and cannot be simulated with the proposed model, or in fact, with the large majority of the models available for steel reinforcing bars.

6. Conclusions

This paper presents a simplified and easy to implement constitutive model to simulate most of the phenomena that characterize the steel reinforcement response under general loading cases. Special attention is drawn to the ultra-low-cycle fatigue effect that occurs when the steel reinforcements experience large inelastic cyclic strains and may result into significant steel resistance and stiffness degradation that may lead to premature collapse by fracture.

The so-called *RSteel* model is completely defined by 10 parameters and is characterized by a bilinear response at first loading, which is followed by a softened branch defined by the well-known Guiffrè-Menegotto-Pinto equation [11, 24], later improved by Filippou *et al.* [10]. A new proposal is presented for the yield surface evolution that allows the consideration of both kinematic and isotropic cyclic hardening observed in the experiments. Moreover, a new definition is presented for the R parameter evolution, which is associated with the curvature of the softened branch. The *RSteel* model includes an innovative and simplified formulation for

considering the fatigue phenomenon for situations in which failure is achieved with less than 50 full cycles with plastic deformation (ultra-low-cycle). This sub-model was designed to be easily implemented in a finite element formulation.

The comparison made with experimental results showed that the *RSteel* model can reproduce the loading and unloading paths for multiple load-reload cycles with a very good accuracy. In addition, it was possible to define the tangent stiffness matrix, which always introduces a significant advantage with respect to the computational efficiency.

The main issues identified for future research are pursuing the model validation with additional experimental results, in particular for cases when failure is achieved with a larger number of cycles, and assessing the model parameters sensitivity through parametric tests. Furthermore, the introduction of steel bar buckling, of strain-rate effects and the possibility of simulating asymmetric tension-compression cycles are also identified as pertinent future work.

7. Acknowledgements

The authors would like to acknowledge and emphasize the importance of the financial support given to this research by *Fundação para a Ciência e a Tecnologia* through the doctoral and postdoctoral grant with references SFRH/BD/21491/2005 and SFRH/BPD/75878/2011, respectively.

8. Appendix

Note: Tables 2, 3 and 4 are to be placed in the Appendix.

References

[1] Aktan, A., Karlsson, B., Sozen, M. A., 1973. Stress-strain relationships of reinforcing bars subjected to large strain reversals. Tech. rep., University of Illinois.

[2] Apostolopoulos, C. A., Papadopoulos, M. P., 2007. Tensile and low cycle fatigue behavior of corroded reinforcing steel bars S400. Construction and Building Materials 21 (4), 855–864.

[3] Brown, J., 1996. Fatigue characteristics of reinforcing bars under simulated seismic loading. Ph.D. thesis, Department of Civil and Environmental Engineering, University of Central Florida.

[4] Brown, J., Kunnath, S. K., 2000. Low cycle fatigue behavior of longitudinal reinforcement in reinforced concrete bridge columns. Tech. rep., Multidisciplinary Center For Earthquake Engineering Research, University at Buffalo, State University of New York.

[5] Chang, G. A., Mander, J. B., 1994. Seismic energy based fatigue damage analysis of bridge columns: Part I - Evaluation of seismic capacity. Tech. rep., Multidisciplinary Center For Earthquake Engineering Research, University at Buffalo, State University of New York.

[6] Coffin, L. F. J., 1954. A study of the effects of cyclic thermal stresses on a ductile metal. Trans. American Society of Mechanical Engineers 76, 931–950.

[7] Crisfield, M. A., 1991. Non-Linear Finite Element Analysis of Solids and Structures - Volume 1: Essentials. John Wiley & Sons Ltd, New York.

[8] Dhakal, R., Maekawa, K., 2002. Modeling of Post-yield Buckling of Reinforcement. Tech. rep., University of Canterbury. Civil and Natural Resources Engineering.

[9] Dodd, L., Restrepo-Posada, J., 1995. Model for Predicting Cyclic Behavior of Reinforcing Steel. Journal of Structural Engineering 121 (3), 433–445.

[10] Filippou, F. C., Popov, E., Bertero, V., 1983. Effects of bond deterioration on hysteretic behavior of reinforced concrete joints. Tech. rep., Earthquake Engineering Research Center, University of California.

[11] Giuffrè, A., Pinto, P., 1970. Il comportamento del cemento armato per sollecitazioni cicliche di forte intensità. Giornale del Genio Civile.

[12] Gomes, A., Appleton, J., 1997. NonLinear Cyclic Stress Strain Relation of Reinforced Bars Including Buckling. Engineering Structures 19 (10), 822–826.

[13] Hawileh, R., Rahman, A., Tabatabai, H., 2010. Evaluation of the low-cycle fatigue life in ASTM A706 and A615 grade 60 steel reinforcing bars. Journal of Materials in Civil Engineering 22 (1), 65–76.

[14] Holmes, J., 2002. Fatigue life under along-wind loading - closed-form solutions. Engineering Structures 24 (1), 109 – 114.

[15] Kemper, F. H., Feldmann, M., 2011. Fatigue life prognosis for structural elements under stochastic wind loading based on spectral methods, Part I: Linear structures. In: Roeck, G. D., Degrande, G., Lombaert, G., Muller, G. (Eds.), Proceedings of the 8th International Conference on Structural Dynamics, EURODYN 2011. Leuven, Belgium, 4-6 July 2011.

[16] Kent, D. C., Park, R., 1973. Cyclic load behaviour of reinforcing steel. Strain 9 (3), 98–103.

[17] Koh, S. K., Stephens, R. I., 1991. Mean stress effects on low cycle fatigue for a high strength steel. Fatigue and Fracture of Engineering Materials and Structures 14 (4), 413–428.

[18] Leslie, P. D., 1974. Ductility of reinforced concrete bridge piers. Tech. rep., University of Canterbury.

[19] Ma, S. M., Bertero, V. V., Popov, E. P., 1976. Experimental and analytical studies on the hysteretic behaviour of reinforced concrete rectangular and T-beams. Tech. rep., Earthquake Engineering Research Center, University of California.

[20] Mander, J., Priestley, M., Park, R., 1984. Seismic design of bridge piers. Tech. rep., University of Canterbury.

[21] Mander, J. B., 1983. Seismic design of bridge piers. Ph.D. thesis, University of Canterbury.

[22] Mander, J. B., Panthaki, F. D., Kasalanati, A., 1994. Low-cycle fatigue behavior of reinforcing steel. Journal of Materials in Civil Engineering 6 (4), 453–468.

[23] Manson, S. S., 1953. Behavior of materials under conditions of thermal stress. In: Heat Transfer Symp. University of Michigan Engineering Research Institute, Ann Arbor, Mich. 9-75.

[24] Menegotto, M., Pinto, P. E., 1973. Method of analysis for cyclically loaded RC plane frames including changes in geometry and non-elastic behavior of elements under combined normal force and bending. In: IABSE Symposium on Resistance and Ultimate Deformability of Structures Acted on by Well Defined Repeated Loads. LNEC, Lisboa.

[25] Monti, G., Nuti, C., 1992. Nonlinear cyclic behavior of reinforcing bars including buckling. Journal of Structural Engineering 118 (12), 3268–3284.

[26] Panthaki, F. D., 1992. Low cycle fatigue behavior of high strength and ordinary reinforcing steels. Ph.D. thesis, State University of New York at Buffalo.

[27] Ramberg, W., Osgood, W., 1943. Description of stress-strain curves by three parameters. Tech. rep., National Advisory Committee for Aeronautics.

[28] Roberti, R., Cornacchia, G., Faccoli, M., 2011. On the extremely low cycle fatigue behavior of the concrete reinforcing bar B450C (FeB44k) steel. In: Convegno Nazionale IGF XXI. Cassino (FR), Italy, pp. 181–190.

[29] Rocha, M., Brühwiler, E., 2012. Prediction of fatigue life of reinforced concrete bridges using Fracture Mechanics. In: Biondini, F., Frangopol, D. (Eds.), Proceedings Bridge Maintenance, Safety, Management, Resilience and Sustainability. Vol. 1. CRC Press/Balkema, London, pp. 3755–3761.

[30] Soltani, A., Harries, K., Shahrooz, B., Russell, H., Miller, R., 2012. Fatigue performance of high-strength reinforcing steel. Journal of Bridge Engineering 17 (3), 454–461.

[31] Suidan, M. T., Eubanks, R. A., 1973. Cumulative fatigue damage in seismic structures. Journal of the Structural Division - ASCE 99 (ST5), 923–941.

[32] Tilly, G. P., 1979. Fatigue of steel reinforcement bars in concrete : A review. Fatigue of Engineering Materials and Structures 2, 251–268.

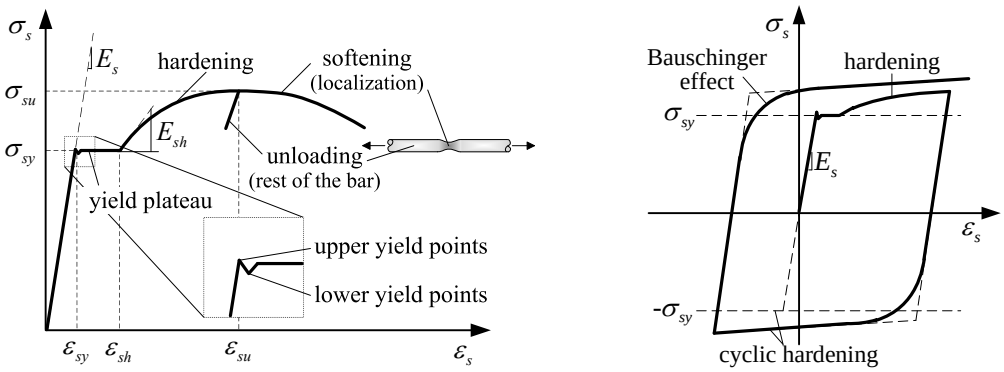

(a) monotonic (hot rolled steel) (b) cyclic

Figure 1: Typical response of reinforcing steel bars on tension tests.

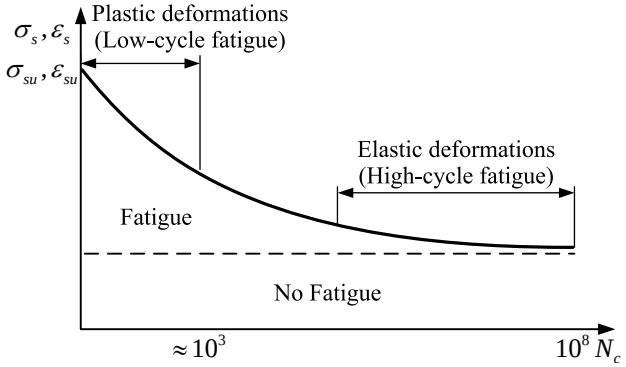

Figure 2: Typical fatigue-life curve for an engineering alloy, after Brown *et al.* [4].

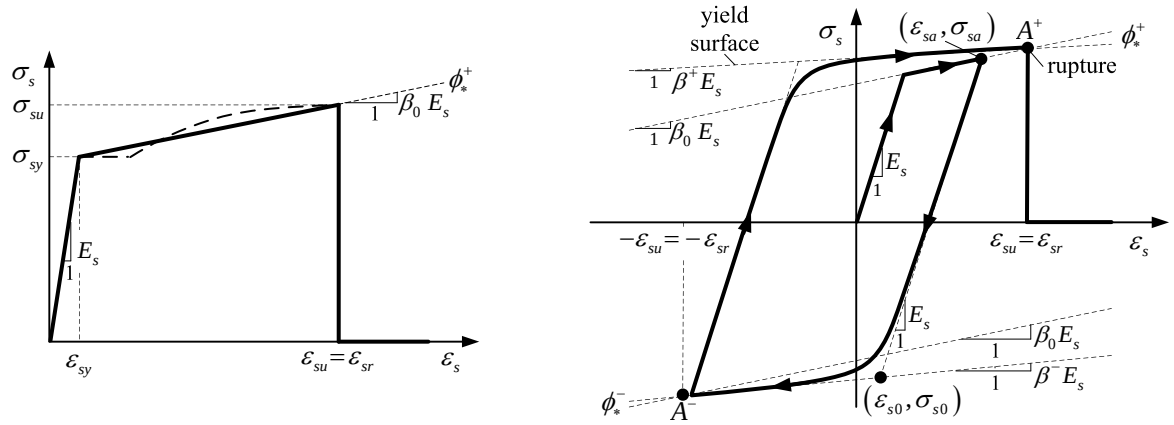

(a) monotonic (b) cyclic

Figure 3: Schematic representation of the *RSteel* model.

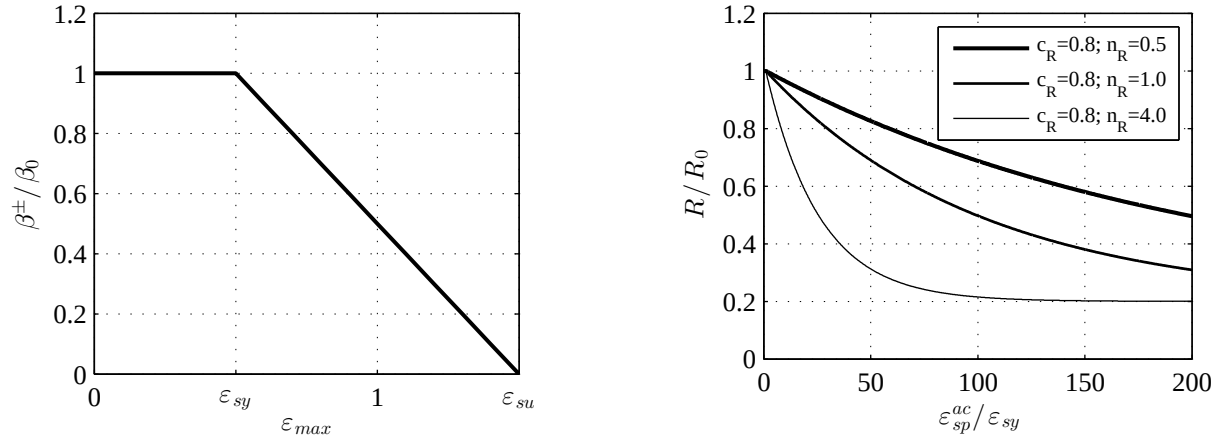

(a) Evolution of the parameter $\beta^{\pm}$

(b) Evolution of the parameter R with c_R and n_R

Figure 4: Model parameters.

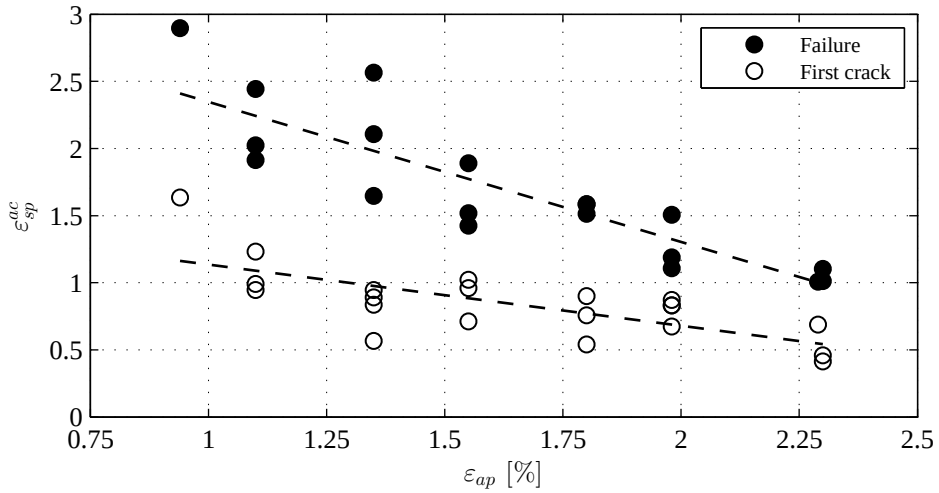

Figure 5: Accumulated plastic strain at the identification of the first crack or at bar failure for the tests performed by Brown *et al.* [4].

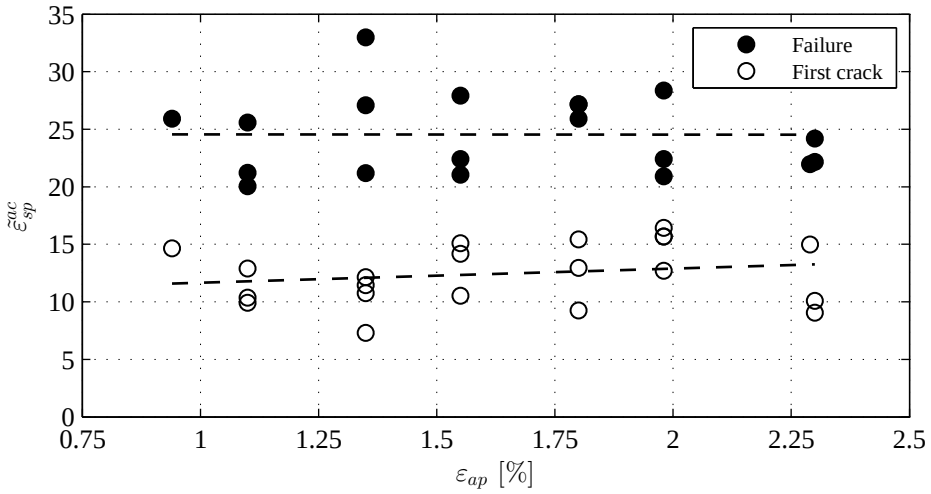

Figure 6: Corrected values of the accumulated plastic strain for the tests performed by Brown *et al.* [4].

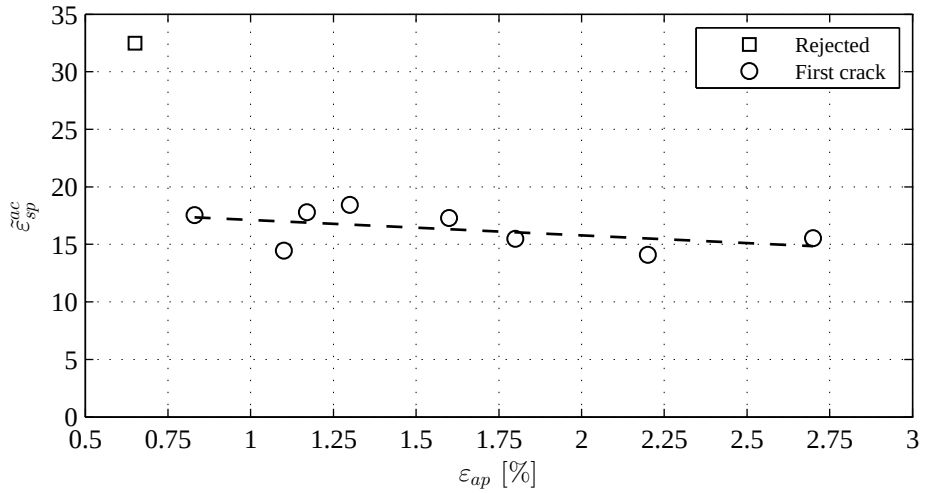

Figure 7: Corrected values of the accumulated plastic strain for the tests performed by Mander *et al.* [22, 26].

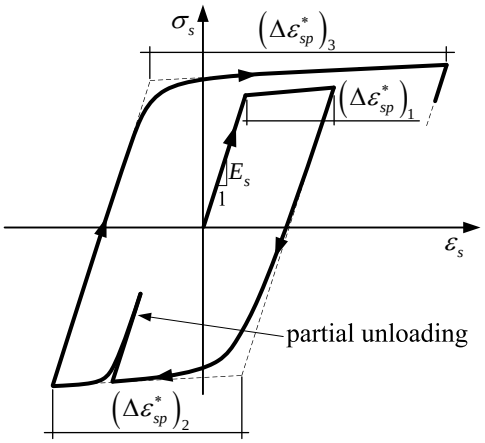

Figure 8: Definition of the accumulated plastic strain.

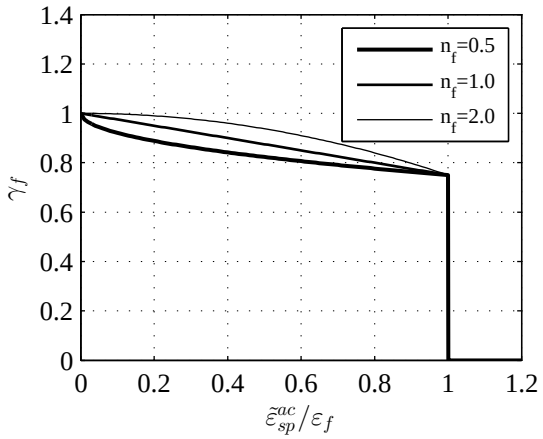

Figure 9: Evolution of the fatigue factor with n_f $\left(c_f = 0.25\right)$.

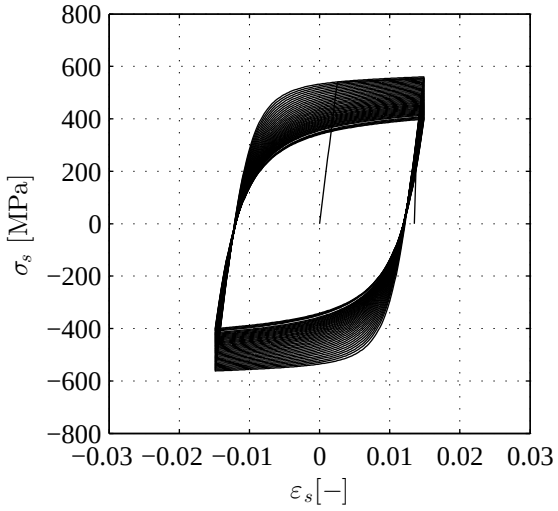

(a) ε_a = 1.50% (*RSteel* model)

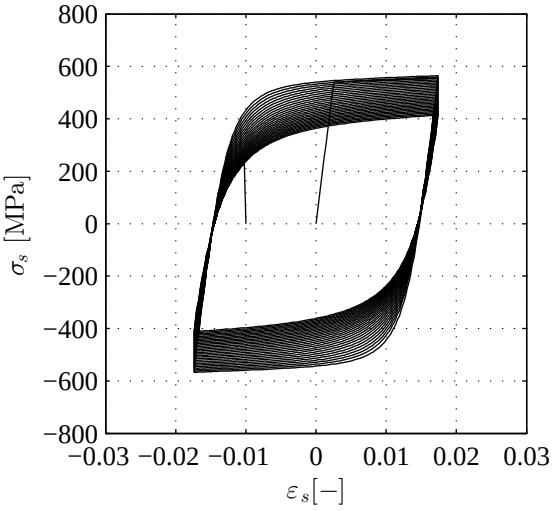

(b) ε_a = 1.75% (*RSteel* model)

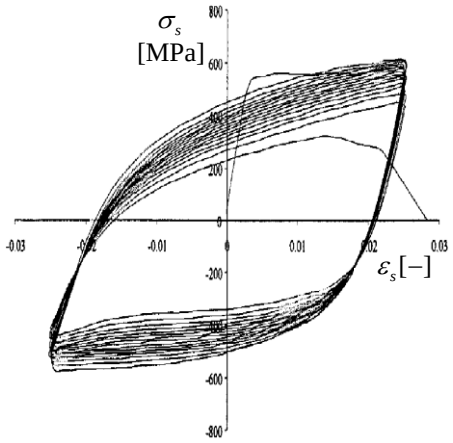

(c) ε_a = 2.50% (Experimental [4])

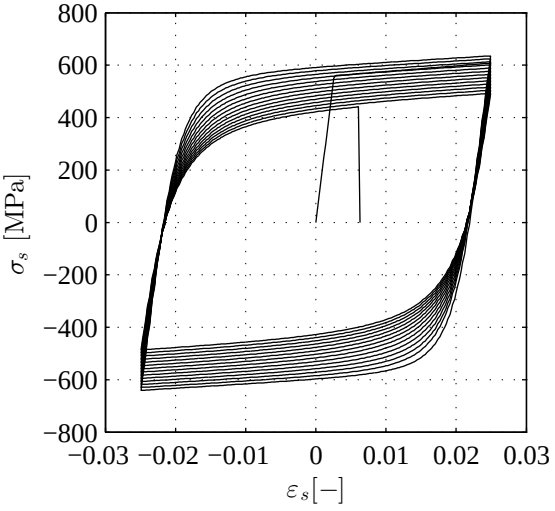

(d) ε_a = 2.50% (*RSteel* model)

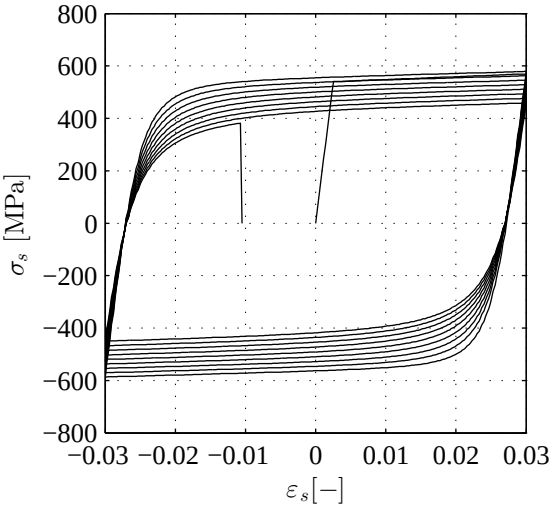

(e) ε_a = 3.00% (*RSteel* model)

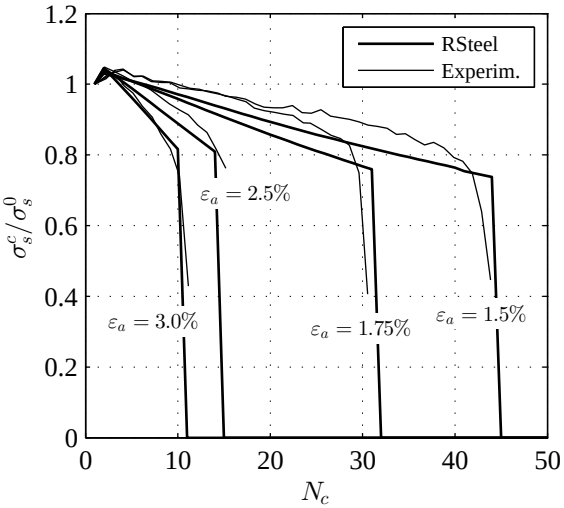

(f) tension peaks at reversal (Experimental [4])

Figure 10: Comparison of the low-cycle fatigue tests performed by Brown *et al.* [4] with the results obtained using the *RSteel* model.

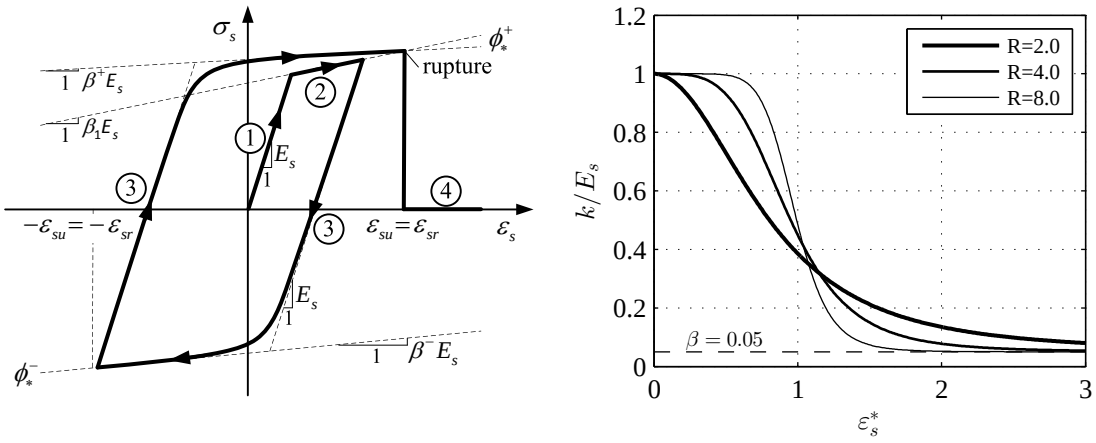

(a) stress-strain branches

(b) influence of the parameter R

Figure 11: Implementation of the *RSteel* model.

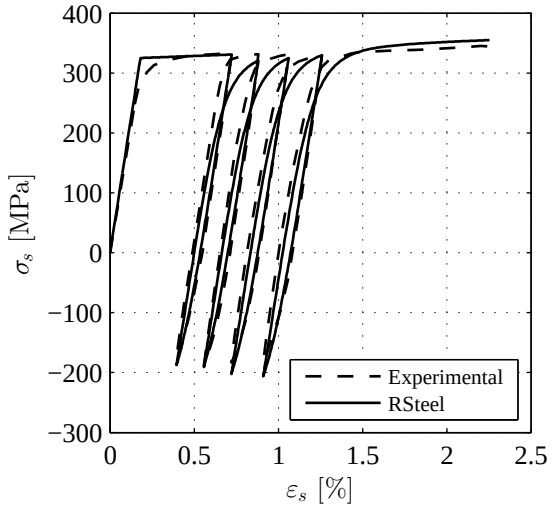

(a) Tests by Kent and Park [16], Spec. 17, after [21]

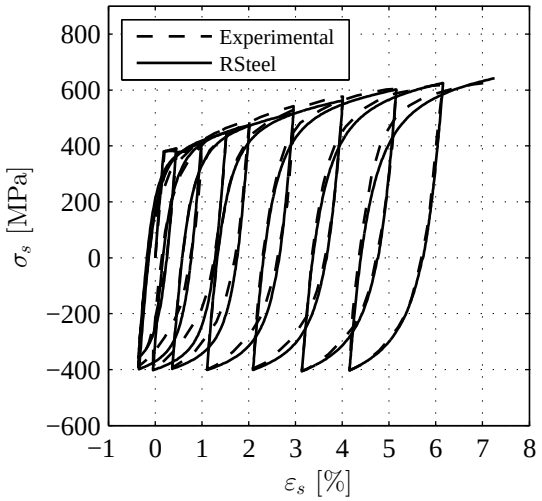

(b) Tests by Leslie [18], Spec. A, after [21]

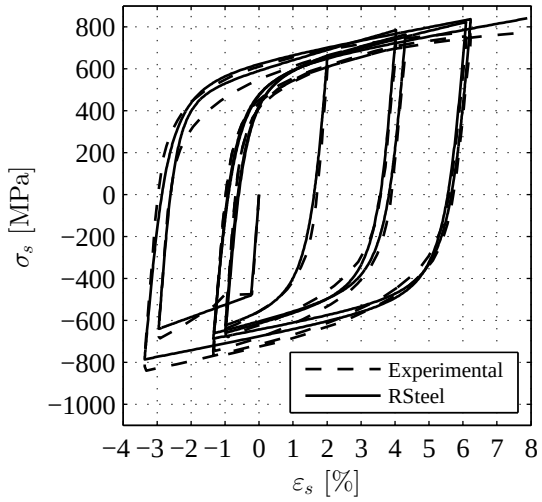

(c) Tests by Aktan *et al.* [1], Test 5, #9 bar

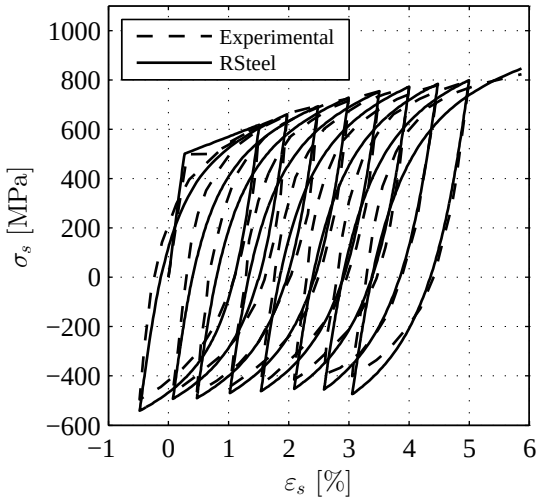

(d) Tests by Aktan *et al.* [1], Test 8, #6 bar

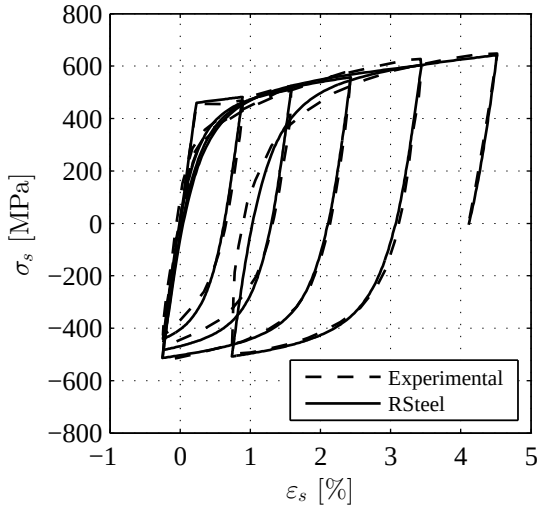

(e) Tests by Ma *et al.* [19], Specimen 3

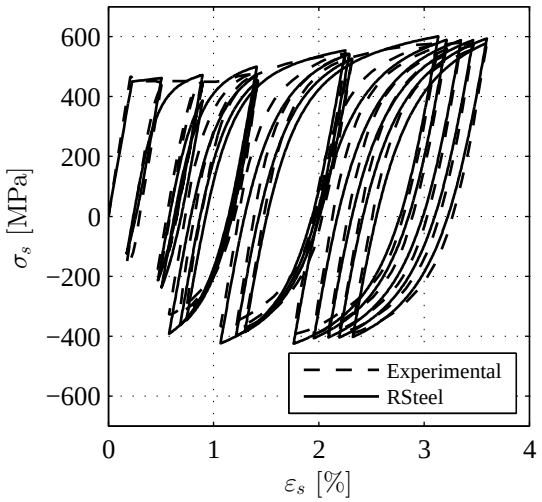

(f) Tests by Ma *et al.* [19], Specimen 2

Figure 12: *RSteel* model - Comparison with experimental results.

Table 1: *RSteel* model parameters.

Parameter	Unit	Domain	Definition
E_s	Pa	$[0, \infty]$	elastic stiffness
σ_{sy}	Pa	$[0, \infty]$	yield stress
β_0	-	$[0, \infty]$	initial hardening factor
ε_{su}	m/m	$\left[\sigma_{sy}/E_s, \infty\right]$	strain at peak stress
R_0	-	$[0, \infty]$	initial value of R
c_R	-	$[0, 1]$	reduction factor of R
n_R	-	$[0, \infty]$	exponent used to control the evolution of R
ε_f	-	$[0, \infty]$	value of $\tilde{\varepsilon}_{sp}^{ac}$ at failure
c_f	-	$[0, 1]$	reduction factor of γ_f
n_f	-	$[0, \infty]$	exponent used to control the evolution of γ_f

Table 2: Results of fatigue tests performed by Brown *et al.* [4]

Specimen	ϕ (mm)	ε_a (%)	ε_{ap} (%)	N_c^{cr}	N_c^f
#21	19	±1.50	1.10	28.0	43.5
#22		±1.75	1.35	15.5	30.5
#23		±2.00	1.55	15.5	24.5
#26		±2.25	1.80	12.5	22.0
#24		±2.50	1.98	8.5	15.0
#25		±3.00	2.30	4.5	11.0
#33	22	±1.25	0.94	43.5	77.0
#32		±1.50	1.10	21.5	46.0
#28		±1.75	1.35	16.5	30.5
#34		±1.75	1.35	17.5	47.5
#27		±2.00	1.55	11.5	23.0
#29		±2.25	1.80	10.5	21.0
#30		±2.50	1.98	10.5	19.0
#35		±2.50	1.98	11.0	19.0
#31		±2.75	2.29	7.5	11.0
#36		±3.00	2.30	5.0	12.0
#43	25	±1.50	1.10	22.5	55.5
#46		±1.75	1.35	10.5	39.0
#44		±2.00	1.55	16.5	30.5
#47		±2.25	1.80	7.5	22.0
#45		±2.50	1.98	10.5	14.0

Table 3: Results of fatigue tests performed by Mander *et al.* [22, 26]

Specimen	ε_a (%)	ε_{ap} (%)	N_c	Failure Criteria
R8	±0.80	0.65	148.0	
R4	±1.00	0.83	49.0	normalized
R10	±1.25	1.10	23.0	tensile stress
R21	±1.34	1.17	25.0	starts dropping
R7	±1.50	1.30	21.0	
R11	±1.75	1.60	13.0	
R5	±2.00	1.80	9.2	tension
R9	±2.50	2.20	5.6	crack
R1	±3.00	2.70	4.1	initialization

Table 4: Model parameters used for computing the stress-strain curves presented in Figure 12.

Parameter	12a	12b	12c	12d	12e	12f
E_s (GPa)	180	210	210	190	200	200
σ_{sy} (MPa)	325	380	480	500	460	450
ε_{su} (%)	18.0	12.0	14.0	8.0	12.0	12.0
β_0 (%)	0.60	1.90	2.80	5.00	1.70	2.10
R_0	4.00	2.50	2.50	1.80	2.50	2.80
c_R	0.60	0.60	0.20	0.20	0.25	0.35
n_R	0.80	0.80	4.00	3.00	4.00	5.00
ε_f	24.50	24.50	24.50	24.50	24.50	24.50
c_f	0.40	0.40	0.30	0.45	0.30	0.35
n_f	0.60	0.60	0.40	0.38	0.75	0.75

Algorithm 1: *RSteel* model state determination.

Initialize: State variables: $\varepsilon_{sa} = \varepsilon_{s0} = \sigma_{sa} = \sigma_{s0} = 0; \beta^{\pm} = \beta_0; R^{\pm} = R_0; \gamma_f = 1.$

For each new load increment (j):

1. **Update**: Strain increment: $\Delta\varepsilon_s = \varepsilon_s - (\varepsilon_s)_{j-1}$.

2. **Update**: Maximum absolute strain: $\varepsilon_{max} = \max\left\{(\varepsilon_{max})_{j-1}, \varepsilon_s)\right\}$.

3. **Compute:** $\beta^{\pm}$ using Equation (5).

4. **If** $\Delta\varepsilon_s(\Delta\varepsilon_s)_{j-1} < 0 \ \wedge \ \varepsilon_{max} > \varepsilon_{sy}$ (def. increment reversal):
   Update: $\varepsilon_{sa} = (\varepsilon_s)_{j-1}$;
   Update: $\sigma_{sa} = (\sigma_s)_{j-1}$;
   Compute: γ_f using Equation (19).

5. **If** $\varepsilon_{sa} = \sigma_{sa} = 0$ (first loading – bilinear branch):
   Compute: $\Phi^{\pm}$ using Equation (6);
   Compute: σ_t using Equation (1);
   If $\sigma_t - \Phi^{+} > 0$:
   Compute: $\varepsilon_p = \varepsilon - \Phi^{+}/E_s$.
   If $\sigma_t - \Phi^{-} < 0$:
   Compute: $\varepsilon_p = \varepsilon - \Phi^{-}/E_s$.

   Else (subsequent loading – softened branch):
   If $\Delta\varepsilon_s \geq 0$, $(\pm \leftarrow +)$; **Else**: $(\pm \leftarrow -)$;
   Compute: $\varepsilon^{\pm}_{s0}$ using Equation (10);
   Compute: $\sigma^{\pm}_{s0} \times \gamma_f$ using Equation (11);
   Compute: ε^{*}_{s} using Equation (8a);
   Compute: R using Equation (12);
   Compute: σ^{*}_{s} using Equation (7);
   Compute: σ_s using Equation (8b);
   Compute: ε_{sp} using Equation (2).

6. **Update**: $\Delta\varepsilon_{sp} = (\Delta\varepsilon_{sp})_{j-1} + \left|\varepsilon_{sp} - (\varepsilon_{sp})_{j-1}\right|$.

7. **If** $\sigma_{j-1}\left\{E_s(\varepsilon_s - \varepsilon_{sp})\right\} \leq 0$ (load reversal):
   Compute: ε^{ac}_{sp} using Equation (14);
   Compute: $\tilde{\varepsilon}^{ac}_{sp}$ using Equation (17);
   Update: $\Delta\varepsilon_{sp} = 0$.

8. **If** $\varepsilon_{max} \geq \varepsilon_{su} \ \vee \ \tilde{\varepsilon}^{ac}_{sp} > \varepsilon_f$ (rupture):
   Update: $\sigma_s = 0$.